Available online at www.sciencedirect.com

ScienceDirect

IFAC Papers Online CONFERENCE PAPER ARCHIVE

IFAC PapersOnLine 55-6 (2022) 496–501

# Coordinated control design for steering and torque-vectoring in Model-Free Control structure

**Tamás Hegedűs** *, **Dániel Fényes** *, **Balázs Németh** *,**, **Zoltán Szabó** *, **Péter Gáspár** *

* *Institute for Computer Science and Control (SZTAKI), Eötvös Loránd Research Network (ELKH), Budapest, Hungary; E-mail: [tamas.hegedus,daniel.fenyes,balazs.nemeth,zoltan.szabo,peter.gaspar]@sztaki.hu*

** *Department of Control for Transportation and Vehicle Systems, Budapest University of Technology and Economics, Stoczek u. 2, H-1111 Budapest, Hungary. E-mail: balazs.nemeth@kjk.bme.hu*

**Abstract:** Model-Free Control (MFC) approach is a novel technique to handle nonlinearities and uncertainties in control systems in order to provide enhanced performance level. The design of MFC is based on an ultra-local model, which is an approximation of the dynamics of the controlled system for a short period of time. This structure also involves a model-based robust control, which guarantees the accurate tracking performance of the closed-loop system. In this paper, a novel technique is proposed for designing the robust control for taking into account the varying characteristics of the ultra-local model. A novel modeling method is presented, which combines the original plant of the controlled system and the ultra-local model. Then, a robust control design is proposed, by which the tracking performance and the robustness of the closed-loop system can be guaranteed. The design steps and effectiveness of the proposed control strategy is demonstrated through a vehicle-oriented control problem using the high-fidelity simulation software, CarMaker.



*Keywords:* model-free control, torque vectoring, automated vehicles, robust control

## 1. INTRODUCTION AND MOTIVATION

In general, the controller design process is carried out based on a mathematical model, by which the behavior of the given system can be described. However, a number of difficulties need to be solved during the modeling phase e.g. nonlinearities, uncertain parameters. Moreover, model inaccuracies may cause performance degradation of the controlled system. These effects can be handled using the Model-Free Control (MFC) structure, in which the control input consists of two parts: the ultra-local model and the baseline controller Fliess and Join (2009). The ultra-local model, which is computed using the measured signals, includes the effect of the uncertainties and the nonlinearities of the system. The main role of the baseline controller is to reach zero tracking error.

Several papers address vehicle-oriented problems using an MFC structure. For example, in Polack et al. (2019) an MFC-based solution is proposed for the longitudinal control of the vehicle. Moreover, MFC is also suitable for the lateral control design of a vehicle Menhour et al. (2019). MFC method can also be used to control the subsystems of the vehicle Plumejeau et al. (2019).

In this paper, an MFC-based solution is proposed for the coordinated control design of torque-vectoring and steering interventions. The combination of the classical steering method and the torque vectoring technique has also been considered in literature. For example, Németh et al. (2019) presents a coordination strategy for an independent steering system and the torque vectoring technique, which aims to maintain the maneuverability of the vehicle in case of actuator failure. A torque vectoring-based backup strategy is proposed by Kirli et al. (2019) for autonomous vehicles equipped with a fully functional steer-by-wire system. A similar method is developed by Mi et al. (2015) using a $\mathcal{H}_\infty$-based robust control approach considering the complete failure of the active front-wheel steering system. The novelty of the proposed MFC-based

⋆ The research was supported by the Ministry of Innovation and Technology NRDI Office within the framework of the Autonomous Systems National Laboratory Program. The paper was partially funded by the National Research, Development and Innovation Office under OTKA Grant Agreement No. K 135512.
The works of Tamás Hegedűs and Dániel Fényes were supported by the ÚNKP-21-3 New National Excellence Program of the Ministry for Innovation and Technology from the source of the National Research, Development and Innovation Fund and by the TKP2021-NKTA-01 NRDIO grant on "Research on cooperative production and logistics systems to support a competitive and sustainable economy".


10.1016/j.ifacol.2022.07.177

approach is hidden in the structure of the control. Since control-loop in MFC contains two controllers, i.e., baseline and ultra-local, it can be used for the separation of the two interventions. Consequently, through the ultra-local control, the performance level of the controlled system can be improved, which provides an enhanced safety level for the vehicle.

The contribution of this paper is twofold. In the first step, the original control structure is augmented with the prior knowledge of the system, which is called the nominal model. Using the nominal model, a nominal ultra-local model can be determined. Moreover, another ultra-local model is computed using the measurable signals of the system. By which, in contrast to the original structure, an error-based ultra-local model is computed using the determined ultra-local models.

Second, a novel robust baseline controller design method is presented, which takes into account the effect of the ultra-local model. The control design is based on an extended modeling process, which represents both, the nominal model of the controlled system, and the effect of the error-based ultra-local model. Then, this model serves as a basis for the robust control design. The control design is based on the $\mathcal{H}_\infty$ technique, while in most of the recent papers PID or LQR methods are used Younes et al. (2016). In this way, the advantages of both methods can be exploited: using the error-based ultra-local, nonlinearities and uncertainties can be taken into account, while the robust control design technique guarantees the tracking performance of the closed-loop system. The modeling and control design phases are presented through a vehicle-oriented control problem, such as trajectory tracking of automated vehicles. In this example, the vehicle has two input signals: steering angle, which is computed by the $\mathcal{H}_\infty$ controller while the differential torque is provided by the error-based ultra-local model. The contribution from the viewpoint of vehicle control is an improved trajectory tracking functionality under critical tire-road conditions.

The paper is divided into 6 sections. In Section 2 the original MFC structure and the calculation of the error-based ultra-local model is presented. Then, in Section 3 combined modeling of the considered system and the error-based ultra-local model is proposed. Section 4 presents the robust control design based on the proposed modeling approach. In order to show the effectiveness and the operation of the proposed method, in Section 5 a simulation example can be found. Finally, in Section 6 the contribution of the paper is summarized.

## 2. STRUCTURE OF CONTROL IN MFC STRATEGY

The main purpose of this section is to give a brief introduction to the MFC structure, more detailed description can be found in Fliess and Join (2009). In the rest of the paper, this structure is called as *original structure*. Moreover, the modification of the original structure, in which the error-based ultra-local model is computed, is also presented.

The main goal of the ultra-local model of the system, is to approximate the system at the given operation point. This model must be recomputed at every sampling time step. The so-called *phenomenological model* can be formulated as d'Andrea Novel et al. (2010):

$$y^{(\nu)} = F + \alpha u, \tag{1}$$

where $F \in \mathbb{R}$ is updated at every time step, and involves the unknown dynamics of the system. Moreover, $y \in \mathbb{R}$ gives the measured output and $\alpha \in \mathbb{R}$ is a design parameter. The $\nu^{th}$ derivative of the system output is denoted by $y^{(\nu)}$. Using (1) the ultra-local model of the system can be computed as:

$$F = y^{(\nu)} - \alpha u. \tag{2}$$

The main goal during the control design is to reach the accurate reference signal ($y_{ref}$) tracking. Using the measured output and the reference signal, the error can be computed as:

$$e^{(\nu)} = y^{(\nu)} - y_{ref}^{(\nu)} = F + \alpha u - y_{ref}^{(\nu)}. \tag{3}$$

Since the minimization of the error ($e^{(\nu)} = 0$) is essential, in steady-state, the control input is calculated as:

$$u = \frac{-F + y_{ref}^{(\nu)}}{\alpha}, \tag{4}$$

where $\nu$ gives the $\nu^{th}$ derivative. It is important to note, that using in (3) the $\nu^{th}$ derivative of the error is minimized. In order to reach the zero tracking error, the control structure is augmented by a feedback controller ($\mathcal{K}(e, \hat{x})$). Using the ultra-local model and the feedback controller, the control input of the system can be calculated as:

$$u = \frac{-F + y_{ref}^{(\nu)}}{\alpha} + \mathcal{K}(e, \hat{x}), \tag{5}$$

where $e$ gives the tracking error, and the states of the system are denoted by $\hat{x}$.

*Improvement of MFC structure with model-based control*

Nevertheless, the given system can be controlled by the original MFC structure, several difficulties come up during the implementation process of the controller (e.g. delays, estimation errors see: Polack (2018)). Moreover, the determination of the feedback gains ( $\mathcal{K}(e, \hat{x})$) is challenging without a prior knowledge of the given system. In this subsection, using a prior knowledge of the system (nominal model), an error-based ultra-local model is computed, by which several effects can be taken into account ( e.g. the unmodeled dynamics, uncertain parameters of the system).

In the modified structure, two different ultra-local models are computed. The first one can be determined using the nominal model and the reference signal, while the second one is calculated using the measured signals of the system. Using the ultra local models, the error based ultra-local model can be determined as:

$$y^{(\nu)} = F + \alpha u, \tag{6a}$$

$$y_{ref}^{(\nu)} = F_{nom} + \alpha u_{nom,ref}, \tag{6b}$$

$$\underbrace{y^{(\nu)} - y_{ref}^{(\nu)}}_{e^{(\nu)}} = \underbrace{F - F_{nom}}_{\Delta} + \underbrace{\alpha u - \alpha u_{nom,ref}}_{\alpha \tilde{u}}, \tag{6c}$$

$$e^{(\nu)} = \Delta + \alpha \tilde{u}, \tag{6d}$$

where $F_{nom}$ is the computed nominal ultra-local model and $u_{nom,ref}$ gives reference input, which can be determined by the nominal model. The control input ($u$) of the

system can be computed using (6), by which $e^{(\nu)} \to 0$ can be guaranteed:

$$u \approx -\frac{\Delta}{\alpha}. \tag{7}$$

Note that in the modified structure of the MFC, some information is used about the system, during the computation of the control signal. The nominal part of the ultra-local model is computed using the nominal model, while the ultra-local model of the system is computed using the measured signals. The deviation between the two model gives the error-based ultra-local model ($\Delta$). Furthermore, using the nominal model, a feedback controller ($\mathcal{K}(e, \hat{x})$) is also designed in order to guarantee zero tracking error. Using (7) and an arbitrary chosen controller, the control input of the system can be calculated as:

$$u = \underbrace{-\frac{\Delta}{\alpha}}_{u_1} \underbrace{-\mathcal{K}(e, \hat{x})}_{u_2}. \tag{8}$$

$u_1$ denotes the control input computed by the error-based ultra-local model, $u_2$ is the control input provided by the baseline controller. Note that in the original concept, the sum of the control inputs is applied to the system. In this paper, the goal is to ensure the stable motion of the vehicle under different circumstances. Therefore, based on the computed error-based ultra-local model a differential torque is calculated, by which the stability of the vehicle can be ensured even on road segments with lower adhesion coefficients.

## 3. COMBINED MODELING OF THE SYSTEM AND THE ULTRA-LOCAL MODEL

In this section, the applied lateral vehicle model is presented. Then, the derived model is augmented with the ultra-local model, which results in an extended state-space representation. This representation serves as the basis of the robust control design.

### *3.1 Formulation of two-wheels bicycle model*

The lateral motion of the vehicle is modeled by the two-wheeled dynamical bicycle model, see Rajamani (2005). The model consists of two main dynamical and one additional kinematic equations:

$$I_z\ddot{\psi} = \left(\delta - \beta - \frac{\dot{\psi} l_1}{v_x}\right) C_1 l_1 - \left(\beta + \frac{\dot{\psi} l_2}{v_x}\right) C_2 l_2 + M_d, \tag{9a}$$

$$m\ddot{y}_p = \left(\delta - \beta - \frac{\dot{\psi} l_1}{v_x}\right) C_1 + \left( - \beta + \frac{\dot{\psi} l_2}{v_x}\right) C_2, \tag{9b}$$

$$\ddot{y}_p = v_x(\dot{\psi} + \dot{\beta}). \tag{9c}$$

where $I_z$ represents the yaw-inertia, $\beta = \frac{\dot{y}_p}{v_x}$ is the side-slip of the vehicle, $\dot{\psi}$ denotes the yaw-rate, $v_x$ is the longitudinal velocity of the vehicle, $m$ is the mass, $C_i$ are the cornering stiffnesses of the front and rear axles, $l_i$ are geometric parameters of the car, $\dot{y}_p$ is the lateral velocity of the vehicle. The system has two control signals: $\delta$ is the steering angle while $M_d$ is the differential torque. The presented lateral vehicle model can be transformed into the following state-space representation, which is formed as:

$$\dot{x}_v = A_v x_v + B_v u_v, \tag{10}$$

$$A_v = \begin{bmatrix} -\frac{l_1^2 C_1 + l_2^2 C_2}{I_z v_x} & -\frac{l_1 C_1 - l_2 C_2}{I_z v_x} & 0 \\ \frac{-l_1 C_1 + l_2 C_2}{m v_x} - v_x & -\frac{C_1 + C_2}{m v_x} & 0 \\ 0 & 1 & 0 \end{bmatrix}, \tag{11a}$$

$$B_v = \begin{bmatrix} \frac{l_1 C_1}{I_z} & \frac{1}{I_z} \\ \frac{C_1}{m} & 0 \\ 0 & 0 \end{bmatrix}. \tag{11b}$$

The state vector $x_v$ consists of the signals $x_v = [\dot{\psi}\ \dot{y}_p\ y_p]^T$. The control inputs of the system are $u_v = [\delta, M_d]^T$.

### *3.2 Extended state-space representation*

The presented state-space representation of the lateral dynamics of the vehicle (11) is extended with the error-based ultra-local model. The following assumptions on the extension are considered.

- The error-based ultra-local model requires a measured output of the controlled system, which is, in this case, the yaw-rate of the vehicle: $y = \dot{\psi}$.
- Moreover, the derivative term ($\nu$) is set to 1, which is the yaw acceleration $\dot{y} = \ddot{\psi}$. Since the yaw-acceleration is not a directly measurable signal, a derivative algorithm is needed, in this case the ALIEN filter is applied for this purpose, see Polack (2018).
- the tuning parameter of the error-based ultra-local model ($\alpha$) is set to a fixed value.
- $\dot{y}_{ref}$ is computed as using the ALIEN filter algorithm and the model-based control input ($u_{nom,ref}$) can be found in Hegedűs et al. (2021).
- The baseline controller is omitted ($\mathcal{K}(e, \hat{x})$=0) during the modeling phase.
- In this specific case, the error-based ultra-local controls the differential torque of the vehicle $M_d$, however it uses the steering angle during the computation. Therefore, the provided control signal must be recalculated to the other control signal. It can be computed from the presented model (11) as $M_d = (l_1 C_1) u_1$.

The goal of the extension of the state-space representation is to include the effect of the error-based ultra-local model in the robust control design. The components of the error-based ultra-local model are handled in the following way: $\dot{y}_{ref} = \ddot{\psi}_{ref}$, and $u_{nom,ref} = \delta_{ref}$ are considered to be external, measurable disturbances of the controlled system. The inclusion of the signals $\ddot{\psi}$ and $u$ are more challenging, because $\ddot{\psi}$ is the derivative of one of the states ($\dot{\psi}$), and $u = \delta$ is the control input. In order to solve this issue a filtered derivative term is applied, which can be built into the state space representation. The derivative term can be of a high order, e.g. Pade Approximation see Brezinski (2002). For the sake of simplicity, in this paper a first-order transfer function is used for this purpose. In case of the signal $\ddot{\psi}$, the following transfer function is used:

$$G_{f,1}(s) = \frac{s}{T_1 s + 1}, \tag{12}$$

where $T_1$ is a design parameter. This transfer function can be transformed into a one dimensional state-space representation, whose matrices are: $A_{f,1} = [\frac{-1}{T_1}]$, $B_{f,1} = [\frac{1}{T_1}]$, $C_{f,2} = [1]$. The filtering term of the signal $\ddot{y}$ is of the form, which means: $A_{f,2} = [\frac{-1}{T_2}]$, $B_{f,2} = [\frac{1}{T_2}]$, $C_{f,2} = [1]$. Note that the robust controller uses only the input signal $\delta$, the other intervention is handled by the error-based ultra-local model, by using the mentioned signals: $[\ddot{\psi}, \ddot{\psi}_{ref}, u, u_{nom,ref}]$.

$$\dot{x}_e = A_e x_e + B_e u_e + B_{e,w} w_e, \tag{13a}$$

$$A_e = \left[\begin{array}{c|c|c} A_v & B_{v,2} & -B_{v,2}/\alpha \\ \hline 0_{1\times 3} & A_{f,1} & -B_{f,1}/\alpha \\ \hline B_{f,2}A_v^{1\times 3} & 0_{1\times 1} & A_{f,2} \end{array}\right], \tag{13b}$$

$$B_e = \left[\begin{array}{c} B_{v,1} \\ \hline B_{f,1} \\ \hline 0_{1\times 1} \end{array}\right], \quad B_{e,w} = \left[\begin{array}{c|c} B_{v,2}/\alpha & -B_{v,2} \\ \hline B_{f,1}/\alpha & -B_{f,1} \\ \hline 0_{1\times 1} & 0_{1\times 1} \end{array}\right], \tag{13c}$$

(13d)

where $u_e = [\delta]$, $x_e^T = [\dot{\psi},\ \dot{y}_p,\ y_p,\ u,\ \ddot{\psi}]$, $w_e^T = [\ddot{\psi}_{ref}, u_{nom,ref}]$ and $A_v^{1\times 3} = e^T A_v$, $e^T = [1, 0, 0]$. $B_{v,1} = [\frac{l_1 C_1}{I_z},\ \frac{C_1}{m},\ 0]^T$, $B_{v,2} = [\frac{l_1 C_1}{I_z},\ 0,\ 0]^T$. The extended state-space representation serves as the basis of the robust control design, which is detailed in the following section.

## 4. CONTROL DESIGN BASED ON THE EXTENDED PLANT

In this section, the robust control design of the extended plant is presented. The main goal of the control design is to guarantee the accurate trajectory tracking of the vehicle while guaranteeing the stable motion of the vehicle. Thus, the performances of the control system are defined as follows:

- Firstly, the main goal of the control system is to guarantee the trajectory tracking of the vehicle, which means that the deviation between the reference and measured lateral position must be minimized:
$$z_1 = y_{p,ref} - y_p, \quad |z_1| \to min! \tag{14}$$
- Secondly, the tracking of of the reference signal must be achieved by using minimal control input, which can be expressed as:
$$z_2 = \delta, \qquad |z_2| \to min! \tag{15}$$

The presented performance requirements can be achieved by using appropriately chosen weighting functions. The augmented plant is shown in Figure 1.

As it can be seen, the augmented plant contains several weighting functions, which serve different purposes. For example, $W_{z,1}$ and $W_{z,2}$ are to guarantee the presented performances. Moreover, the weighting functions $W_{w,1}$, $W_{w,2}$ and $W_{w,3}$ scale the noises on the measured signals. The goal of $W_{ref,1}$ is to weight reference signal in order to facilitate smooth trajectory tracking. Functions $W_{u_{nom,ref}}$ and $W_{\ddot{\psi}_{ref}}$ scale the external signals from the error-based ultra-local model.

The state-space representation of the augmented plant can be written as:

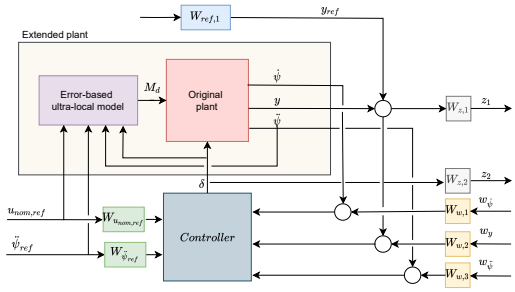


Fig. 1. Scheme of augmented plant

$$\dot{x}_e = A_e x_e + B_e u_e + B_{e,w} w_e, \tag{16a}$$
$$z_e = C_{e,1} x_e + D_{e,1} u_+, \tag{16b}$$
$$y_e = C_{e,2} x_e + D_{e,2} w_{e,2}, \tag{16c}$$

$w_{e,2}$ contains the noises of the measured signals.

The control design is based on the robust $\mathcal{H}_\infty$ approach. The main goal of the control design is to find a controller $K_e$, which can guarantee that the closed-loop system is asymptotically stable and satisfies the following inequality:

$$||\Gamma_{z,e}, w_{e,3}||_\infty < \gamma, \tag{17}$$

where $\Gamma$ is the co-sensitivity function from the disturbances $w_{e,3}$ to the performances $z_e$, and $\gamma$ is a predefined positive real value. This optimization problem can be solved by using Linear Matrix Inequalities (LMI)-based approaches, see Scherer and Weiland (2000).

The whole control system is depicted in Figure 2. The error-based ultra-local model creates an inner loop, which provides an additional steering angle. This additional steering angle aims to adjust the dynamics of the controlled system to the nominal model. The robust $\mathcal{H}_\infty$-based controller makes up the outer loop, whose goal is to guarantee the trajectory tracking of the vehicle, and, in parallel, to ensure the stability of the closed-loop system.

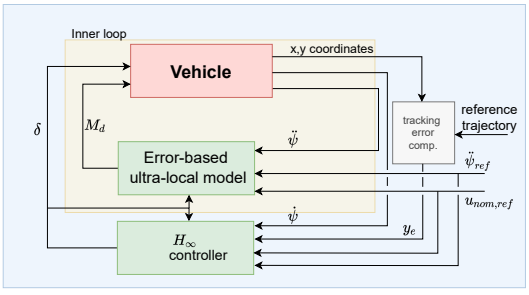


Fig. 2. Architecture of the control system

## 5. SIMULATION RESULTS

In this section, the proposed control algorithm is evaluated through complex simulation scenarios, which are performed using the vehicle dynamics simulation software, CarMaker. The goal of the simulation examples is to show, that performance of trajectory tracking through the proposed method, under various friction coefficients can be guaranteed. The results are compared to the operation of an $\mathcal{H}_\infty$ controller, in which the nonlinear tyre-road characteristics as an uncertainty is taken into account. The uncertainty of this $\mathcal{H}_\infty$ controller through the frequency domain analysis of various simulation scenarios is formulated Gáspár et al. (2017).

This simulation section presents two different test scenarios. In the first scenario, the algorithm is tested for an emergency situation, in which the controlled vehicle starts to slip suddenly, while the straight motion of the vehicle must be guaranteed. This scenario represents a skid-pad test, which means that a lateral force is applied at the rear tyres of the vehicle as a disturbance to destabilize its motion. In the second simulation, the vehicle must perform the tracking of reference trajectory, i.e., the path of Silverstone Racing Track. The longitudinal velocity of the vehicle is selected using the built-in driver model of CarMaker. During the test scenarios the maximum value of the longitudinal velocity is set to $25m/s$.

### *5.1 Skid-pad test*

In this subsection, the results of the skid-pad test are presented. At the beginning of the test, the vehicle starts from $0m/s$ and accelerates to $14m/s$. After the vehicle reaches the predefined velocity value, the longitudinal forces are set to zero. During the tracking, i.e., stabilization process of the motion, only the lateral controller of the vehicle is used. In the test scenarios, the lateral forces are set to $F_s = \{3500,\ 4000,\ 4250,\ 4500\}N$. The lateral error is computed from the yaw-angle and the lateral position of the vehicle using a predictive approach, by which the reaction time can be increased. In Figure 3, the measured velocity and the characteristics of the applied lateral force can be seen.

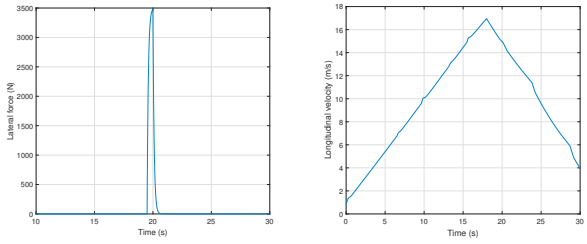


(a) Applied lateral force (b) Velocity of the vehicle

Fig. 3. The lateral force and velocity of the vehicle

The lateral displacement during the test scenarios is presented in Figure 4. The friction coefficient is set to 0.4 in this test scenario.

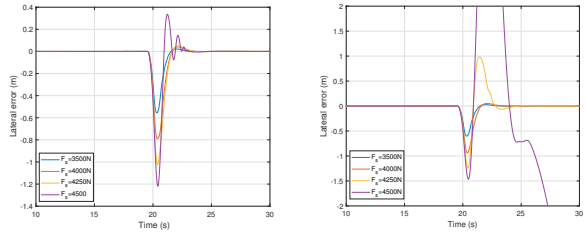


(a) With differential torque (b) Without differential torque

Fig. 4. Lateral displacement of the vehicle

It can be seen in Figure 4 that the displacement of the vehicle increases with the increase of the lateral force. Without the differential torque, the vehicle nearly loses its stability for $4250N$ lateral force. Moreover, the algorithm cannot stabilize the motion of the car for $4500N$ lateral force. Using the proposed method, the vehicle remains stable for $4250N$ lateral force and its motion can be stabilized for $4500N$. In Figure 5 the measured yaw-rate is presented.

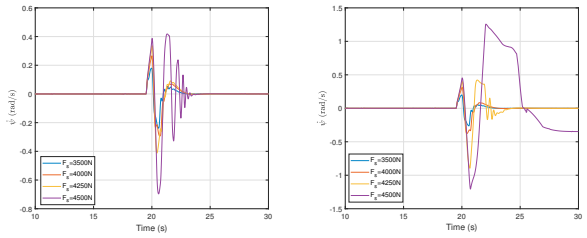


(a) With differential torque (b) Without differential torque

Fig. 5. The measured yaw-rates of the vehicle

Figure 5(a) shows that using the proposed method, the motion of the vehicle can be stabilized even at high yaw-rate values, which is generated by the lateral force. Finally, the differential torque values are presented in Figure 6.

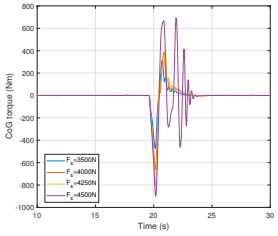


Fig. 6. Differential torque of the vehicle

It can be seen that the computed differential torque values remain in an acceptable range. Moreover, the computed torque values increase together with the lateral force. In this subsection, the effectiveness of the proposed method was presented for skid-pad test scenarios. In the following subsection, the vehicle is driven along a predefined trajectory and the results are compared to a nominal controller.

### *5.2 Trajectory tracking for various friction coefficients*

In this subsection, the tracking performances of both control methods are compared to each other. During the test scenarios, the friction coefficient of the given track decreases until the control algorithm loses its stability. The goal is to show that using the proposed method, the stable motion can be guaranteed even at low friction coefficient values. The lateral error values can be seen in Figure 7.

It can be seen in Figure 7, the vehicle controlled by the baseline $\mathcal{H}_\infty$ controller, loses its stability when the friction coefficient is set to 0.6. However, using the proposed error-based ultra-local control method, the tracking performances are maintained. The lateral error values are nearly the same during the test scenarios. This can be explained by the fact that the goal of the differential torque is to guarantee the stable motion of the vehicle. However, the accurate trajectory tracking is performed using the $\mathcal{H}_\infty$ controller. The maximum value of the lateral error is under $0.5m$ in the most of the simulation time using the

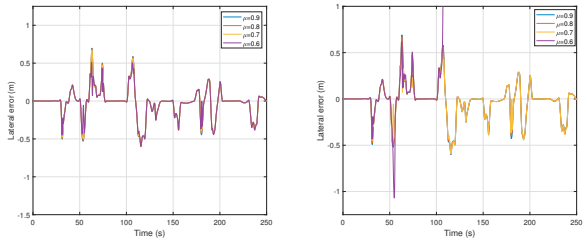


(a) With differential torque (b) Without differential torque

Fig. 7. Lateral error values during test scenarios

proposed method, which is a reasonable value considering that the vehicle is close to its physical limits. In Figure 8, the yaw-rate of the vehicle can be seen for the case, when the differential torque is applied to the vehicle.

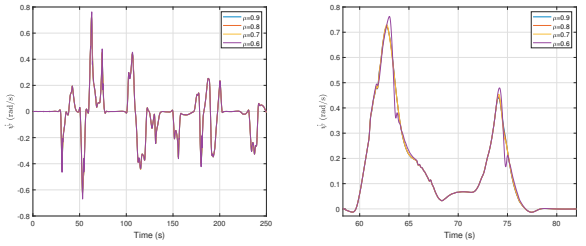


(a) Differential torque (b) Highlighted segment

Fig. 8. Measured yaw-rate value of the vehicle

The maximum value of the yaw-rate reaches $0.7 rad/s$, which is also near to the possible peak value of a road vehicle. Using the proposed method, this value can be reached in the case when the friction coefficient is set to 0.6. It is important to note that during normal traffic situations a road vehicle does not reach these acceleration and yaw-rate values. However, the goal is to demonstrate the effectiveness of the proposed control method even in the highly nonlinear operation range of a car. Moreover, the computed differential torque is presented in Figure 9.

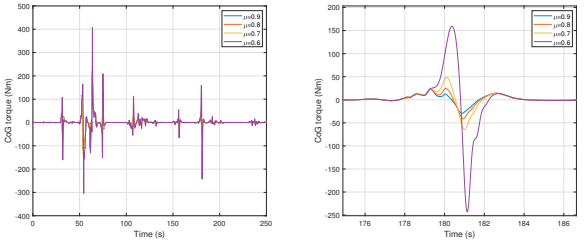


(a) Whole track (b) Highlighted segment

Fig. 9. Differential torque during the test scenario

Figure 9 shows the computed differential torque for the different friction coefficients. It can be seen that the computed torque increases with the decrease of the friction coefficient. Furthermore, the same yaw-rate value can be reached even for low friction coefficients.

## 6. CONCLUSIONS

In this paper, a novel control approach has been presented, which combines ultra-local and robust control methods. The original plant of the controlled system has been extended with the effect of the ultra-local model, which was used to enhance the peformances of the closed-loop system. Then, $\mathcal{H}_\infty$-based robust controller has been designed using the extended plant. The main goal of the robust control design was to guarantee the accurate tracking performances. The proposed control algorithm has been applied to a vehicle-oriented control problem. In this example, the system had two control inputs: steering angle and the differential torque. The steering angle has been computed by the robust controller while the differential torque has been provided by the error-based ultra-local model. The efficiency of the presented algorithm has been demonstrated through two simulation example, which were performed in the high-fidelity simulation software, CarMaker.

## REFERENCES


Brezinski, C. (2002). *Padé Approximations*, 87–134. Springer US, Boston, MA.

d'Andrea Novel, B., Fliess, M., Join, C., Mounier, H., and Steux, B. (2010). A mathematical explanation via 'intelligent' PID controllers of the strange ubiquity of pids. *Proc. 18th Mediterranean Conference on Control and Automation*, 395–400.

Fliess, M. and Join, C. (2009). Model-Free Control and intelligent PID controllers: Towards a possible trivialization of nonlinear control? *Proc. 15th IFAC Symposium on System Identification, Saint-Malo, France*, 42, 1531–1550.

Gáspár, P., Szabó, Z., Bokor, J., and Németh, B. (2017). *Robust Control Design for Active Driver Assistance Systems: A Linear-Parameter-Varying Approach*. Springer International Publishing.

Hegedűs, T., Fényes, D., Németh, B., and Gáspár, P. (2021). Improving sustainable safe transport via automated vehicle control with closed-loop matching. *Sustainability*, 13(20).

Kirli, A., Chen, Y., Okwudire, C.E., and Ulsoy, A.G. (2019). Torque-vectoring-based backup steering strategy for steer-by-wire autonomous vehicles with vehicle stability control. *IEEE Transactions on Vehicular Technology*, 68(8), 7319–7328.

Menhour, L., d'Andrea Novel, B., Fliess, M., Gruyer, D., and Mounier, H. (2019). An efficient model-free setting for longitudinal and lateral vehicle control: Validation through the interconnected Pro-SiVIC/RTMaps prototyping platform. *IEEE Transactions on Intelligent Transportation Systems*, 19, 461–475.

Mi, T., Li, C., Hu, C., Wang, J., Chen, N., and Wang, R. (2015). Robust $\mathcal{H}_\infty$ output-feedback yaw control for in-wheel-motor driven electric vehicles with differential steering. In *2015 54th IEEE Conference on Decision and Control (CDC)*, 1521–1526.

Németh, B., Fényes, D., Gáspár, P., and Bokor, J. (2019). Coordination of independent steering and torque vectoring in a variable-geometry suspension system. *IEEE Transactions on Control Systems Technology*, 27(5), 2209–2220.

Plumejeau, B., Delprat, S., and Keirsbulck, L. (2019). model-free active flow control of a simplified car model. *IFAC-PapersOnLine*, 52(5), 115–120. 9th IFAC Symposium on Advances in Automotive Control AAC 2019.

Polack, P. (2018). Consistency and stability of hierarchical planning and control systems for autonomous driving [dissertation]. *PSL Research University*.

Polack, P., Delprat, S., and dAndrea Novel, B. (2019). Brake and velocity Model-Free Control on an actual vehicle. *Control Engineering Practice*, 92, 1–8.

Rajamani, R. (2005). Vehicle dynamics and control. *Springer*.

Scherer, C. and Weiland, S. (2000). *Lecture Notes DISC Course on Linear Matrix Inequalities in Control*. Delft University of Technology, Delft, Netherlands.

Younes, Y.A., Drak, A., Noura, H., Rabhi, A., and El Hajjaji, A. (2016). Robust Model-Free Control Applied to a Quadrotor UAV. *Journal of Intelligent and Robotic Systems*, 84, 37 – 52.